Supporting Information

Phase-engineered two-dimensional MoO_3/MoS_2 hybrid nanostructures enable efficient indoor organic photovoltaics

Muhammad Ahsan Saeed[a, 1], Muhammad Faizan[b, 1], Tae Hyuk Kim[a], Hyungju Ahn[c], *Ji-Young Kim*[d], Kyung-Wan Nam[b, *], Jae Won Shim[a, *]

[a]School of Electrical Engineering, Korea University, Seoul 02841, Republic of Korea
[b]Department of Energy & Materials Engineering, Dongguk University, Seoul 04620, Republic of Korea
[c]Pohang Accelerator Laboratory, POSTECH, Pohang, 37673, Republic of Korea
[d]Advanced Analysis & Data Center, Korea Institute of Science and Technology (KIST), Seoul 02792, South Korea

*Corresponding authors.
E-mail address: knam@dongguk.edu (K.-W. Nam)
E-mail: jwshim19@korea.ac.kr (J. W. Shim)

[1]Muhammad Ahsan Saeed and Muhammad Faizan contributed equally to this work.

Experimental Details

FDTD Simulation

Optical simulations were performed to obtain the highest J_{SC} value using Maxwell equation-based FDTD simulations (Lumerical Inc., Republic of Korea). A conventional plane-wave source was used to send waves to the photovoltaic device structure. Periodic boundary conditions were assumed on the x-axis and y-axis, whereas perfect matching-layer boundary conditions were estimated along the z-axis. A 3D frequency-domain power monitor was used to quantify the optical absorption in the PM6:Y6: TMSs active layers. A laboratory-made script was used to determine the maximum simulated J_{SC} values under indoor illumination conditions.

Charge Mobility Measurements

Hole- and electron-only OPV devices were constructed using the device structures ITO/2PACz/active layer/MoO_x/Ag and ITO/ZnO/active layer/PDINO/Al, respectively. The hole and electron charge mobilities were estimated using the Mott–Gurney expression:

$$J = \frac{9}{8}\varepsilon_0\varepsilon_r\mu\frac{V^2}{L^3}$$

where J denotes current density, ε_0 is the permittivity of free space (8.85×10^{-12} C·V^{-1}·m^{-1}), ε_r is the relative permittivity of the transport medium (assuming that of 3.0), μ is the charge carrier mobility, V is the internal potential in the device, and L is the thickness of the active layer.

Parasitic Resistance Analysis

The equivalent circuit diode model can be solved analytically using the Shockley equation, and the related photovoltaic parameters J_{SC} and V_{OC} can be expressed as follows:

$$J_{sc} = -\frac{1}{1+\frac{R_s}{R_P}}\left\{J_{ph} - J_o\left(exp\left(\frac{|J_{sc}|R_sA}{\frac{nkT}{e}}\right) - 1\right)\right\} \quad \textbf{(Eq. S1)}$$

$$V_{OC} = n\frac{kT}{e}ln\left\{1 + \frac{J_{ph}}{J_o}\left(1 - \frac{V_{OC}}{J_{ph}R_PA}\right)\right\} \quad \textbf{(Eq. S2)}$$

where J_{ph} denotes the photocurrent density, J_o is the reverse saturation current density, R_S and R_P are the parasitic series and shunt resistances, respectively, e is the elementary charge, n is the ideality factor, T is the temperature, k is the Boltzmann constant (8.617×10^{-5} eV/K), and A is the active area of the OPV.

Similarly, FF ($J_{max}\times V_{max}/J_{SC}\times V_{OC}$) can be expressed as a function of the normalized V_{OC} ($v_{OC} = eV_{OC}/nkT$), normalized R_S ($r_S = R_S/R_{CH}$), and normalized R_P ($r_P = R_P/R_{CH}$), where the characteristic resistance (R_{CH}) is defined as $V_{OC}/(J_{SC}A)$. From this, the semi-empirical expression obtained for FF is given as

$$FF = \left\{\frac{v_{OC} - ln(v_{OC} + 0.72)}{(v_{OC} + 1)}\right\}(1 - 1.1r_s) + 0.19{r_s}^2$$

$$\left\{1 - \frac{(v_{OC} + 0.7)\left\{\frac{v_{OC} - ln(v_{OC} + 0.72)}{v_{OC} + 1}\right\}(1 - 1.1r_s) + 0.19{r_s}^2}{v_{OC} \qquad\qquad r_P}\right\}$$

$$\left(0 \leq r_s + \frac{1}{r_P} \leq 0.4\right) \qquad \textbf{(Eq. S3)}$$

Supporting Figures and Tables

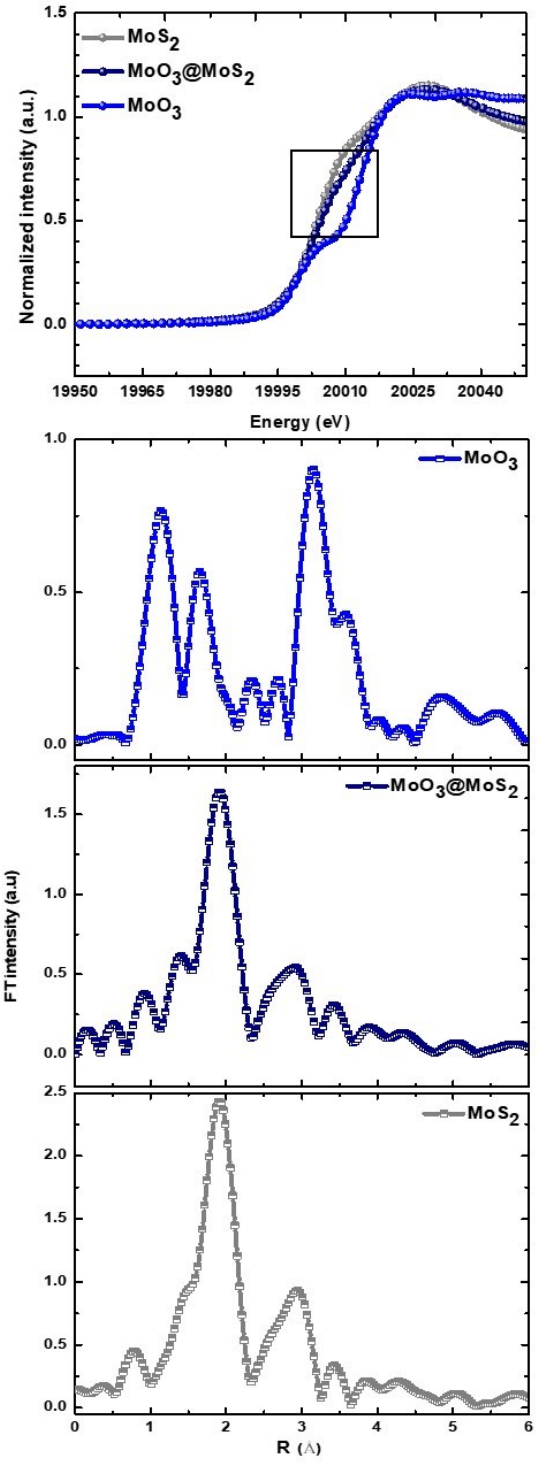

Figure S1. Mo K-edge (a) XANES and (b) FT-EXAFS spectra of MoS_2, MoO_3/MoS_2, and MoO_3.

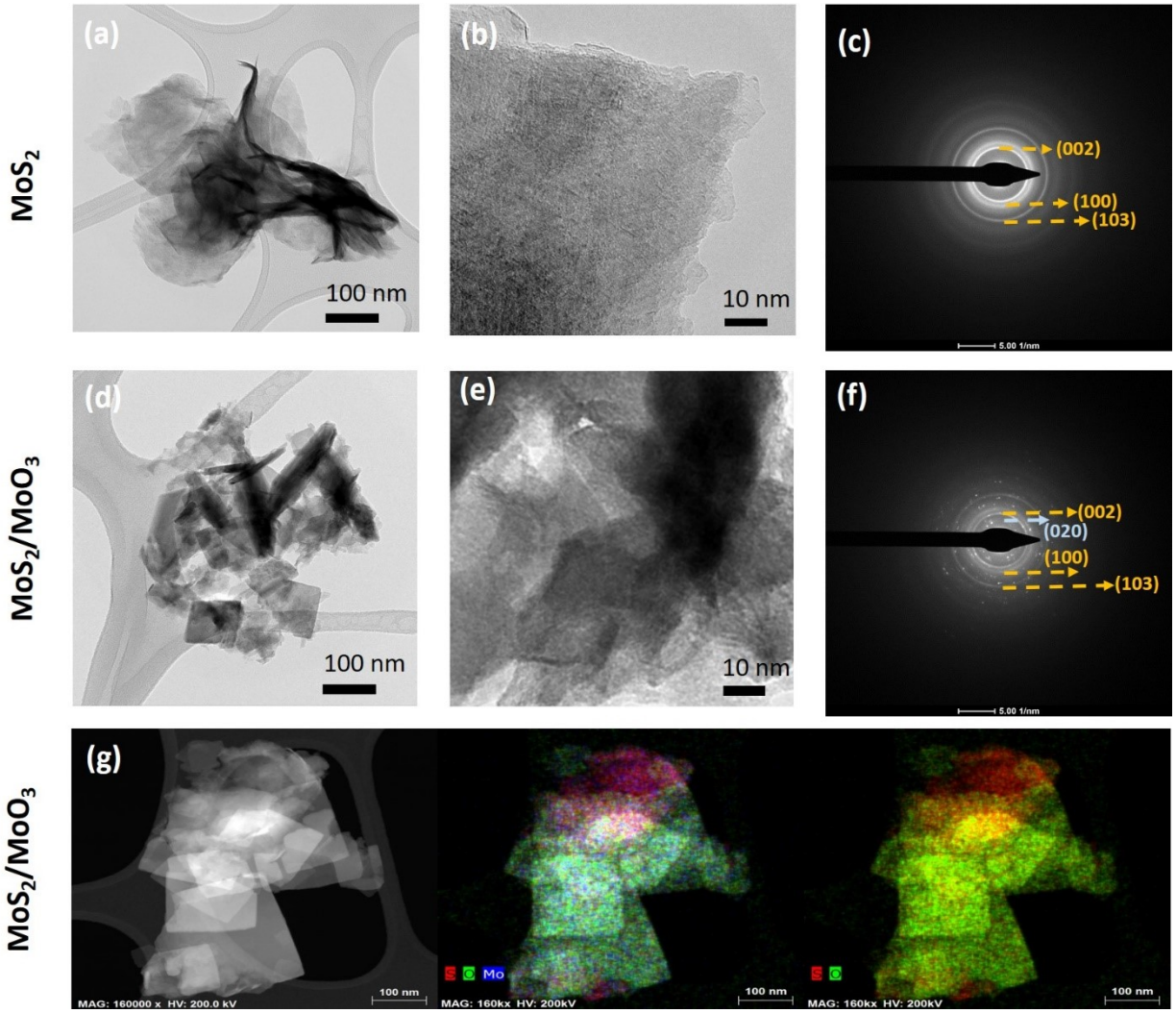

Figure S2. TEM images corresponding SAED pattern of (a–c) MoS_2 and (d–f) MoO_3/MoS_2. (g) TEM-EDS mapping of MoO_3/MoS_2.

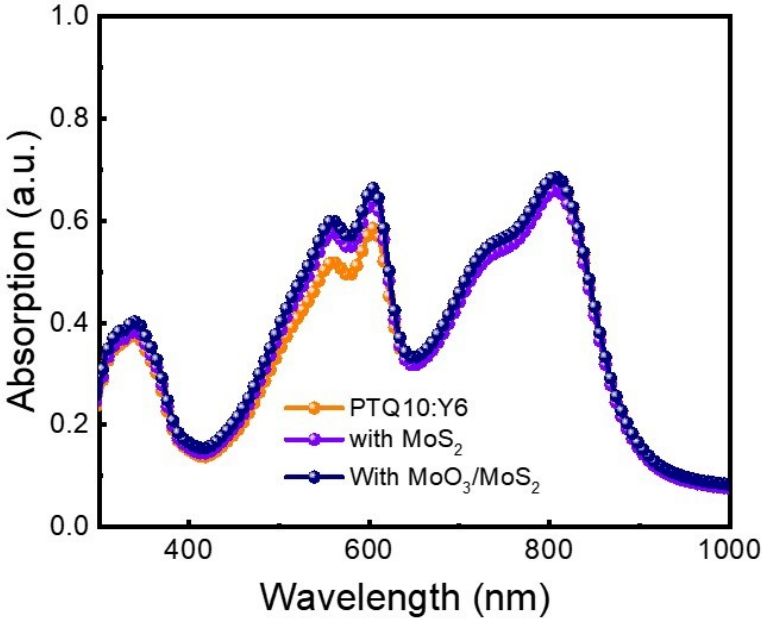

Figure S3. UV-vis absorption of PTQ10:Y6 OPVs doped with TMSs.

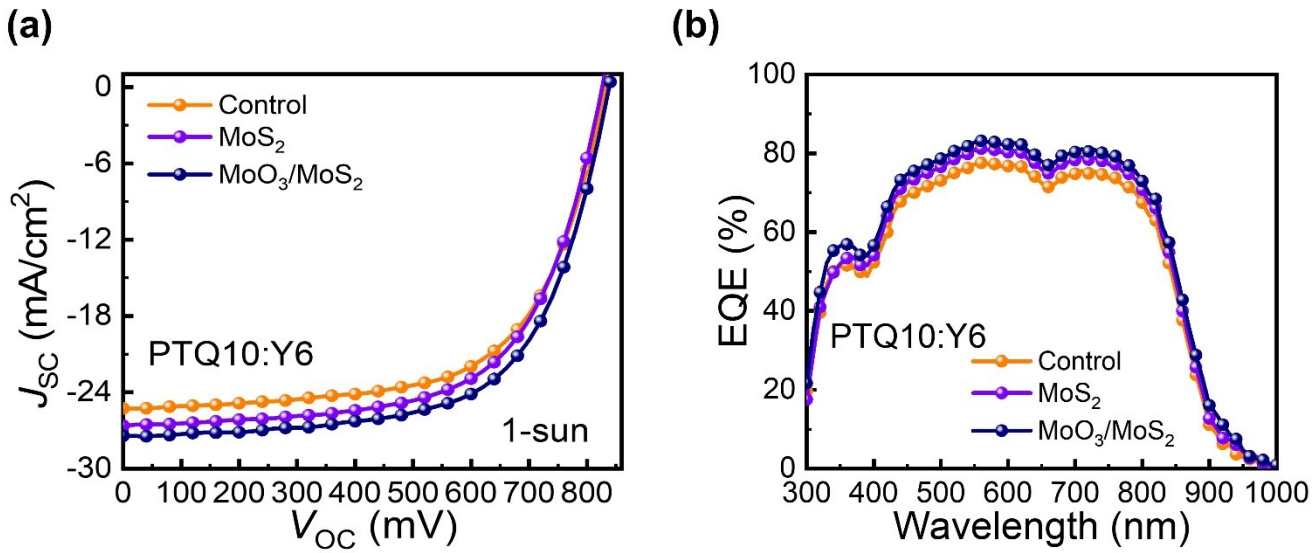

Figure S4. (a) *J-V* curves and (b) EQE spectra of PTQ10:Y6 OPV devices.

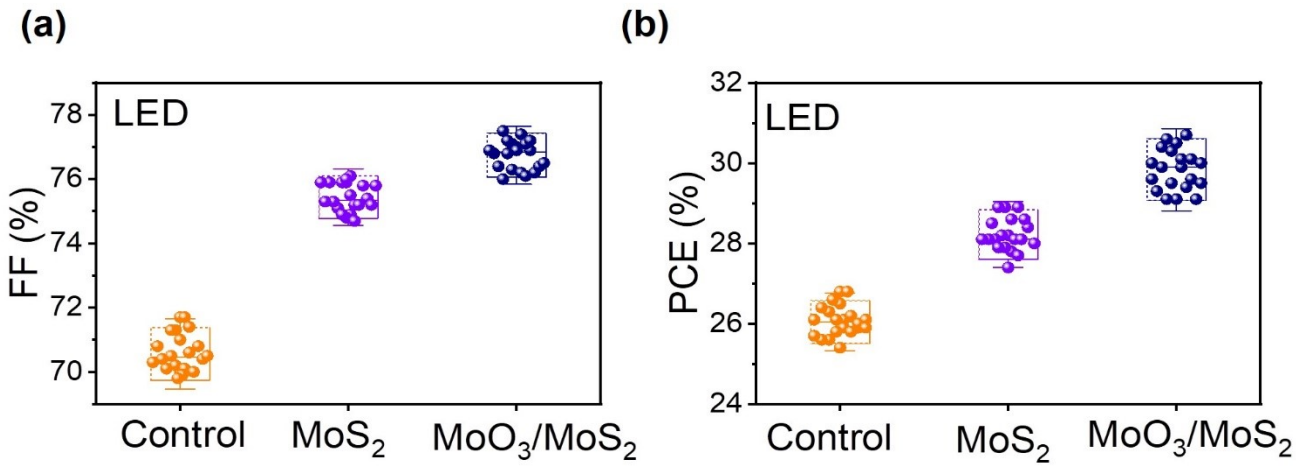

Figure S5. Statistics of photovoltaic parameters (FF and PCE) of OPVs under LED lamp.

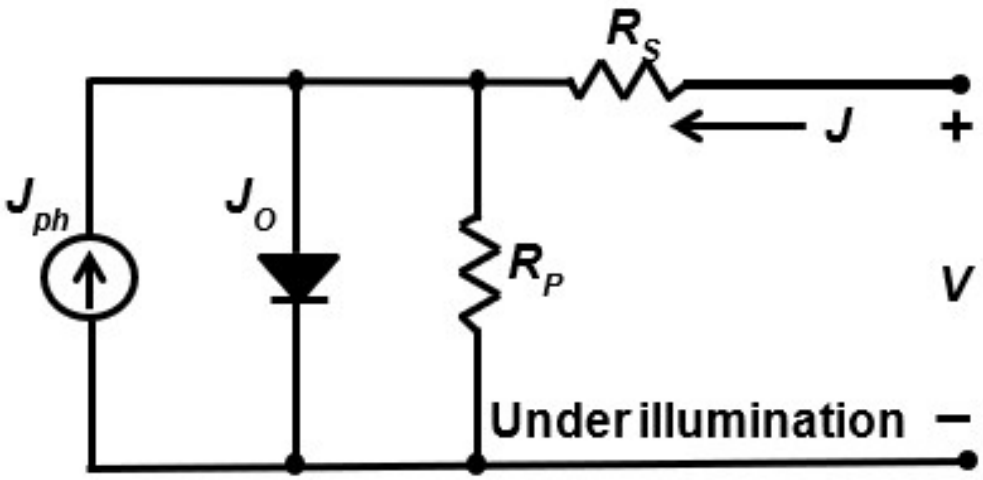

Figure S6. Single-diode equivalent circuit model.

Table S1. Parasitic resistances of OPVs under LED and 1-sun illumination conditions.

	LED 1000-lx			1-sun		
Devices type	r_S	r_P	R_{CH}	r_S	r_P	R_{CH}
Control	0.1206	29.363	115008	0.0149	0.6716	7048
MoS_2	0.1169	48.472	109112	0.0166	0.7462	6790
MoO_3/MoS_2	0.1288	59.642	105071	0.0142	0.5971	6699

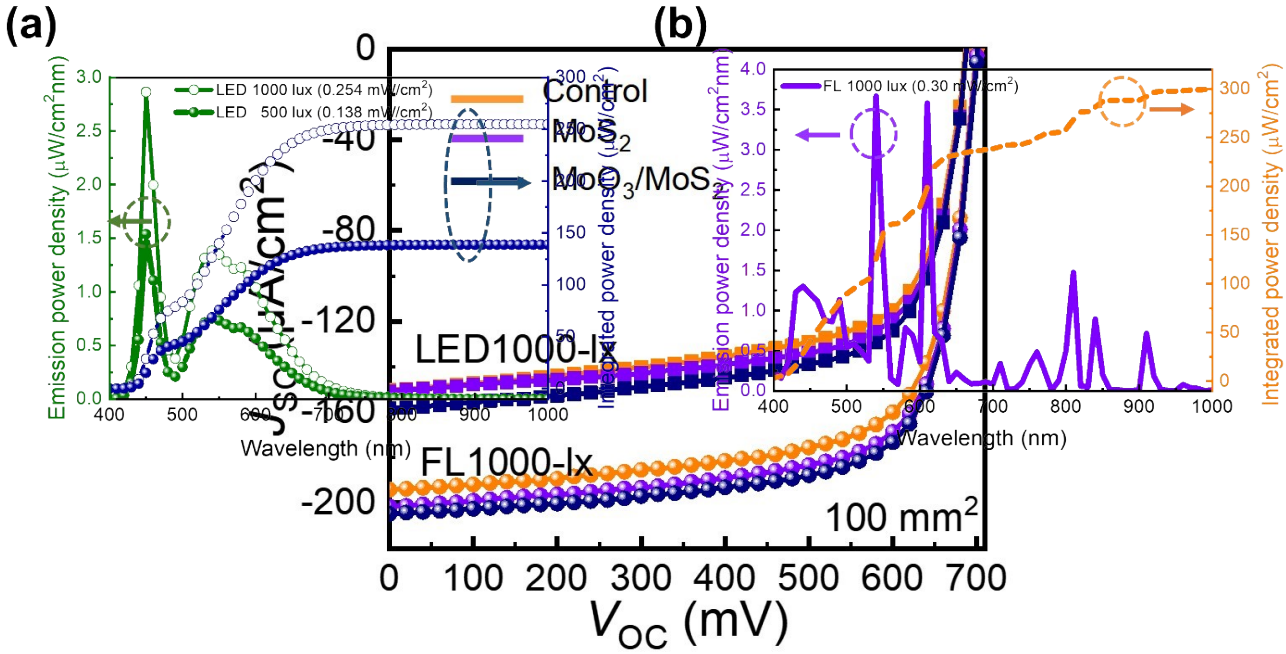

Figure S7. *J–V* curves of OPVs (area: 100 mm2) under LED and FL lamps.

Figure S8. Emission power and integrated power spectra of a LED and FL illumination.

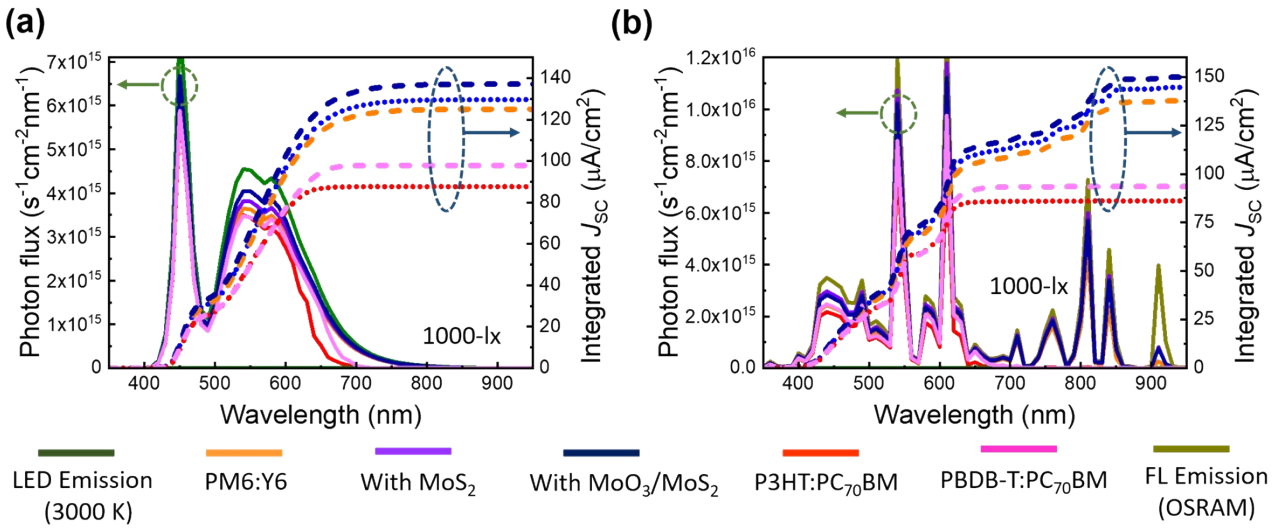

Figure S9. Photon flux and integrated J_{SC} of OPVs under LED and FL illumination.

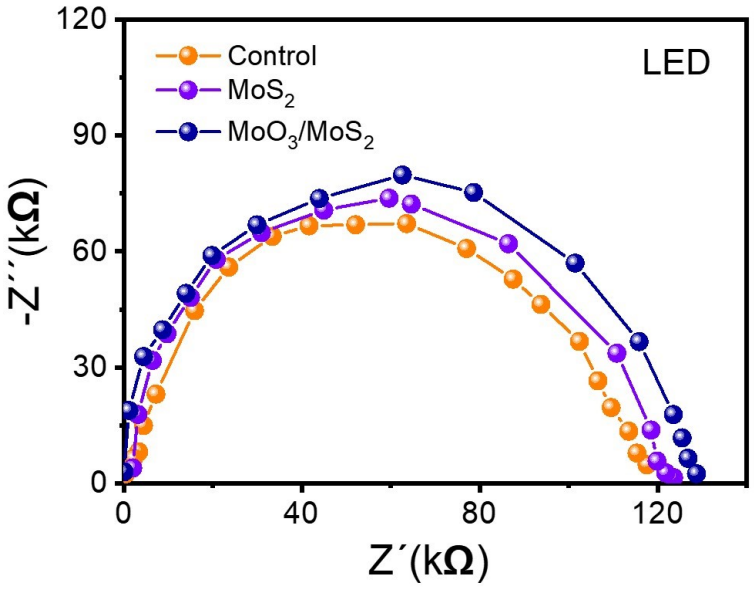

Figure S10. Electrochemical impedance spectroscopy (EIS) plot of OPV devices.

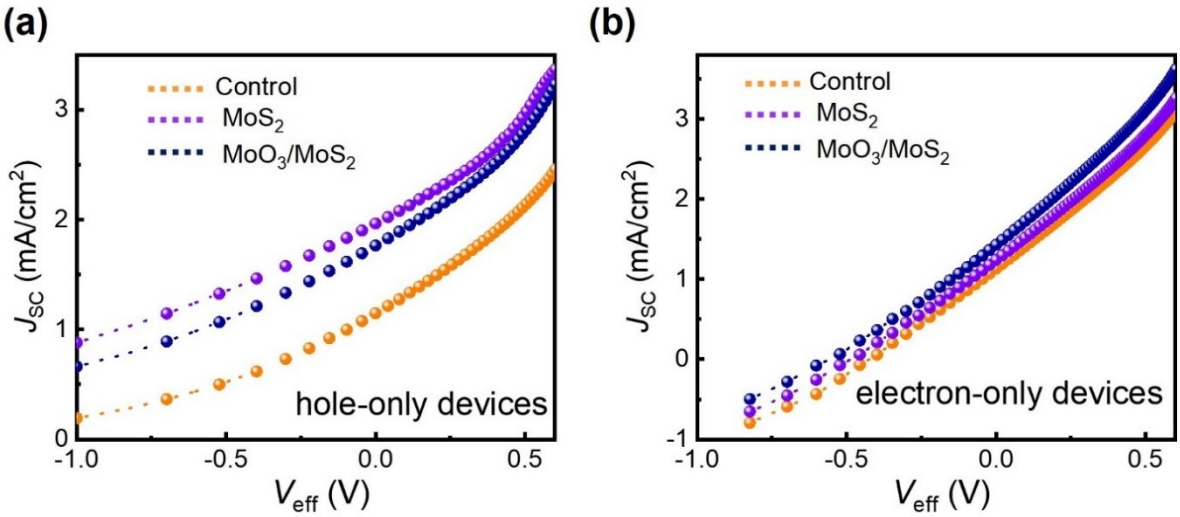

Figure S11. Fitted *J–V* curves for charge mobilities. (a) hole-only devices. (b) electron-only devices.

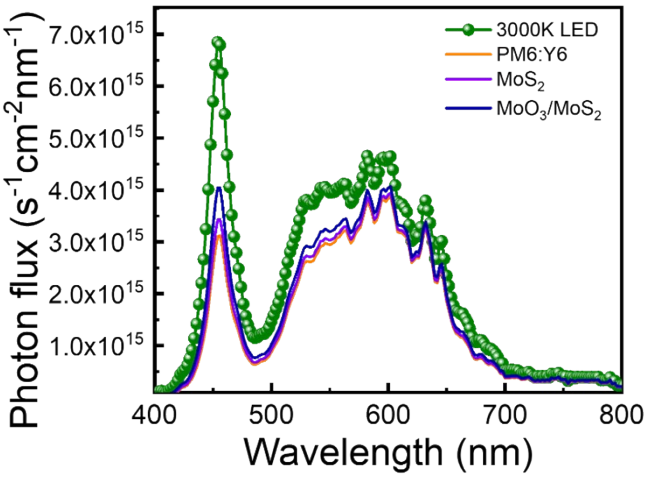

Figure S12. Spectral match of OPVs with LED illumination.

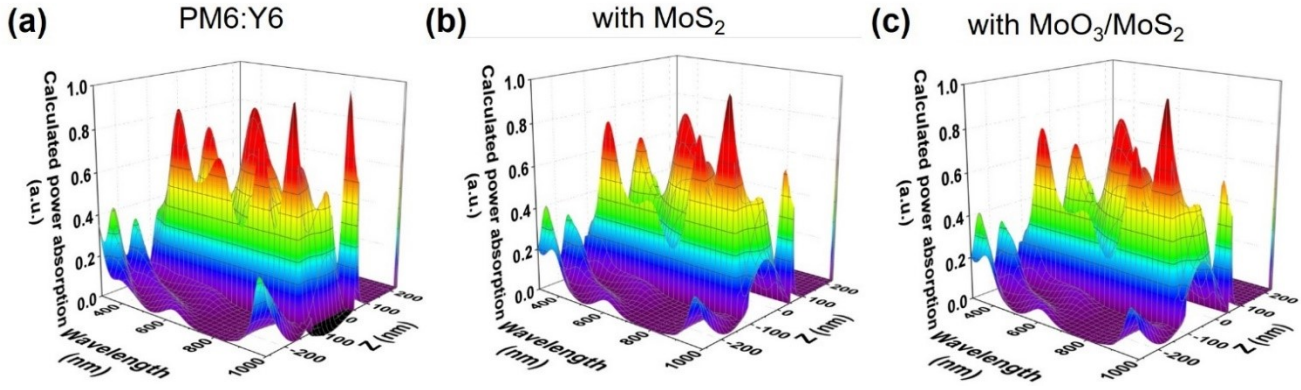

Figure 13. Power absorption density profiles of OPVs calculated using FDTD simulation.

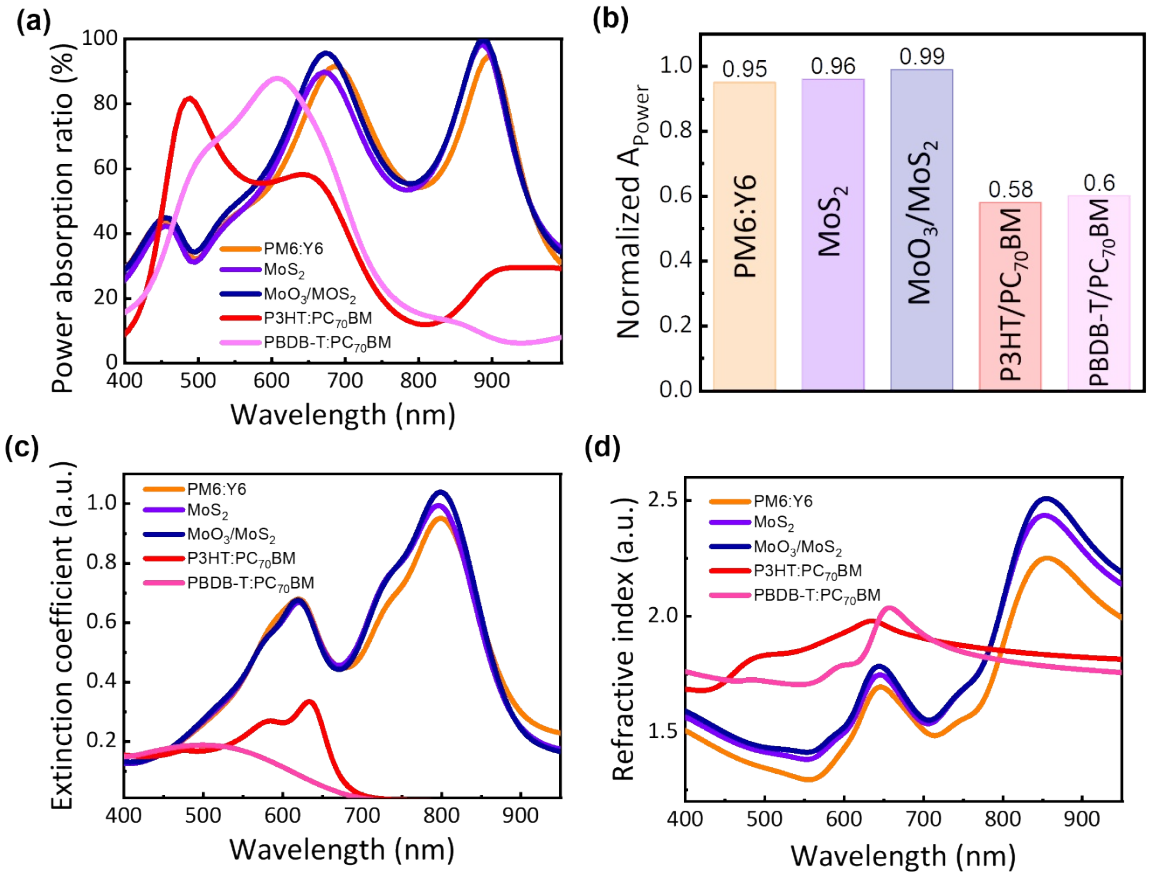

Figure S14. (a) Calculated power absorption ratios of OPVs with different active layers, (b) Normalized absorption power, (c) extinction coefficient, and (d) refractive index.

Table S2. A summary of recently reported photovoltaic performances under a halogen lamp (1000-lx).

Ref	Active layer	V_{OC} (mV)	J_{SC} (μA/cm^2)	FF (%)	P_{max} (μW/cm^2)
[1]	PDTBTBz-2F$_{anti}$:PC$_{71}$BM	809	116.8	70.2	66.3
[1]	P3HT:PC$_{71}$BM	486	71.8	71.0	24.8
[1]	PBDB-T:PC$_{71}$BM	669	108.3	71.0	51.4
[1]	PTB7:PC$_{71}$BM	576	171.4	67.4	66.5
[2]	PBDB-T:IDIC	710	202.7	65.0	94.1
[2]	PBDB-T:IDICO1	770	252.4	66.0	102.1
[2]	PBDB-T:IDICO2	770	271.2	63.0	141.4
[3]	PM6:Y6	741	649.5	69.7	335.1
[3]	PM6:Y6:MXene	751	656.7	74.2	373.3
[4]	PM6:Y6	720	454.2	77.7	254.1
[4]	PM7:IT-4F	750	309.8	72.6	168.7
[4]	PTB7-Th:IEICO-4F	630	403.2	69.8	177.3
[5]	PBDB-T: *m*-ITIC-O-EH	711	198.7	64.9	95.6
[5]	PBDB-T: PC70BM	562	87.6	60.6	31.9
[6]	PM6:PM7:Y6:PCBM	708	551	73.1	280
[7]	PBDB-T:BTA3	1050	289.2	52.4	159.1
[7]	PBDB-TF:BTA3	1140	180.4	54.3	111.7
[7]	PBDB-TCl:BTA3	1180	138.2	43.6	71.1
This work	PM6:Y6:MoS$_2$	755	683	77.1	397.5
This work	PM6:Y6:MoO$_3$/MoS$_2$	761	692	78.1	412.2

Table S3. Ideal current densities of OPVs under 1000-lx LED lamp, calculated by FDTD simulation.

1000-lx LED (P_{in}: 0.254 mW/cm^2)			
		Thickness (nm)	**J_{ph}, ideal**
Narrow bandgap active layers	PM6:Y6	151	140.7
	with MoS$_2$	150	149.9
	with MoO$_3$/MoS$_2$	149	153.6
Wide bandgap active layers	P3HT:ICBA	150	109.2
	P3HT:PC$_{70}$BM	150	119.8
	PBDB-T:PC$_{70}$BM	150	127.1
	P3HT:ICBA (actual thickness)[1]	125	109.2
	P3HT:PC$_{70}$BM (actual thickness)[1]	150	121.1
	PTB7:PC$_{70}$BM (actual thickness)[1]	140	140.5
	PBDB-T:PC$_{70}$BM (actual thickness)[1]	120	132.8

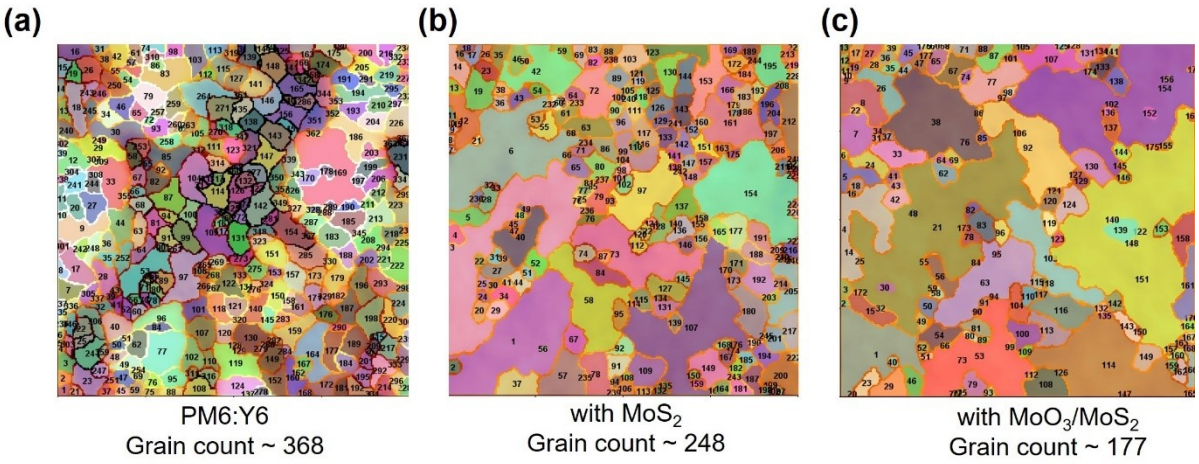

Figure S15. 2D AFM grain-count images of thin film blends measured by Watershed Algorithm.

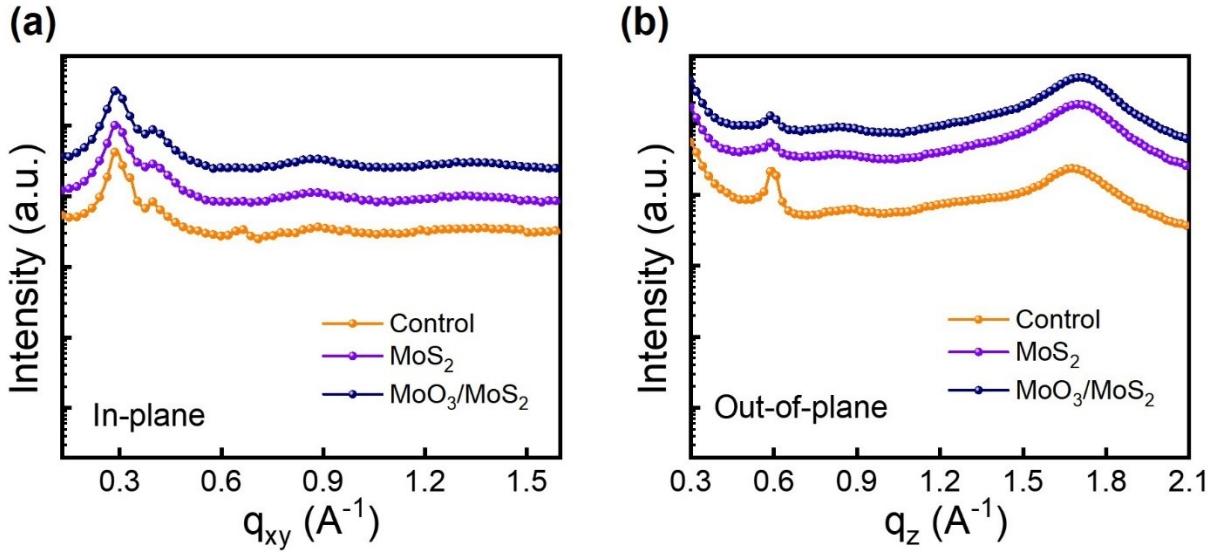

Figure S16. Intensity profiles of active layers blend. (a) In-plane direction. (b) Out-of-plane direction.

Table S4. Extracted parameters of active layers blend from GIWAXS measurements.

Sample	Lamella stacking			π-π stacking		
	[a] $q_{xy}(100)$ (A^{-1})	[b] $d_{lamellar}$ (nm)	[c] CCL (nm)	$q_z(010)$ (A^{-1})	$d_{\pi-\pi}$ (nm)	CCL (nm)
Control	0.2262	22.75	70.98	1.712	3.75	21.25
MoS_2	0.2291	21.62	80.05	1.724	3.70	22.90
MoO_3/MoS_2	0.2305	21.54	86.66	1.739	3.67	23.54

[a]Peak position calculated from original GIWAXS data

[b]Intermolecular distance d = 2π/q

[c]Crystal coherence length (L_C) was calculated using the Scherrer equation, L_C = 2πK/FWHM.

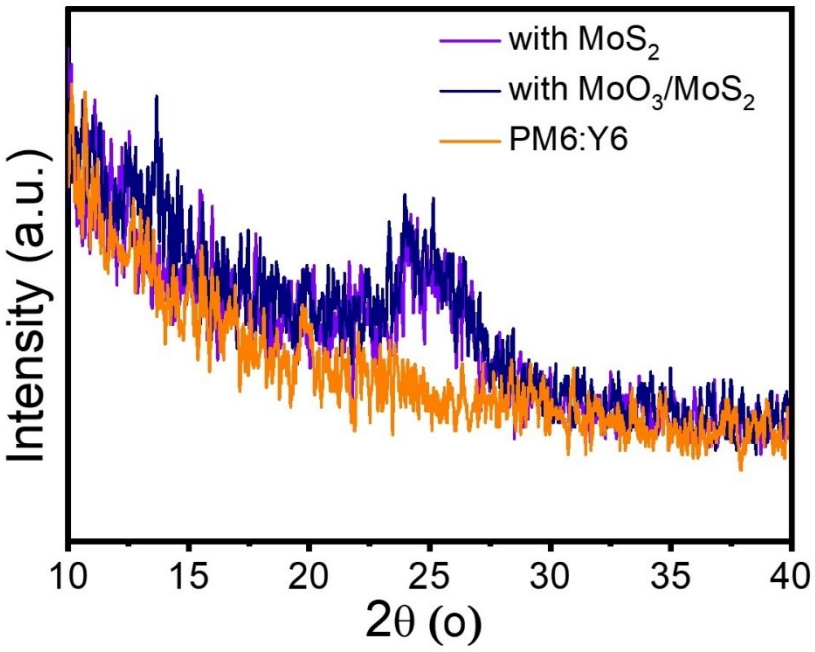

Figure S17. XRD figure of OPVs.

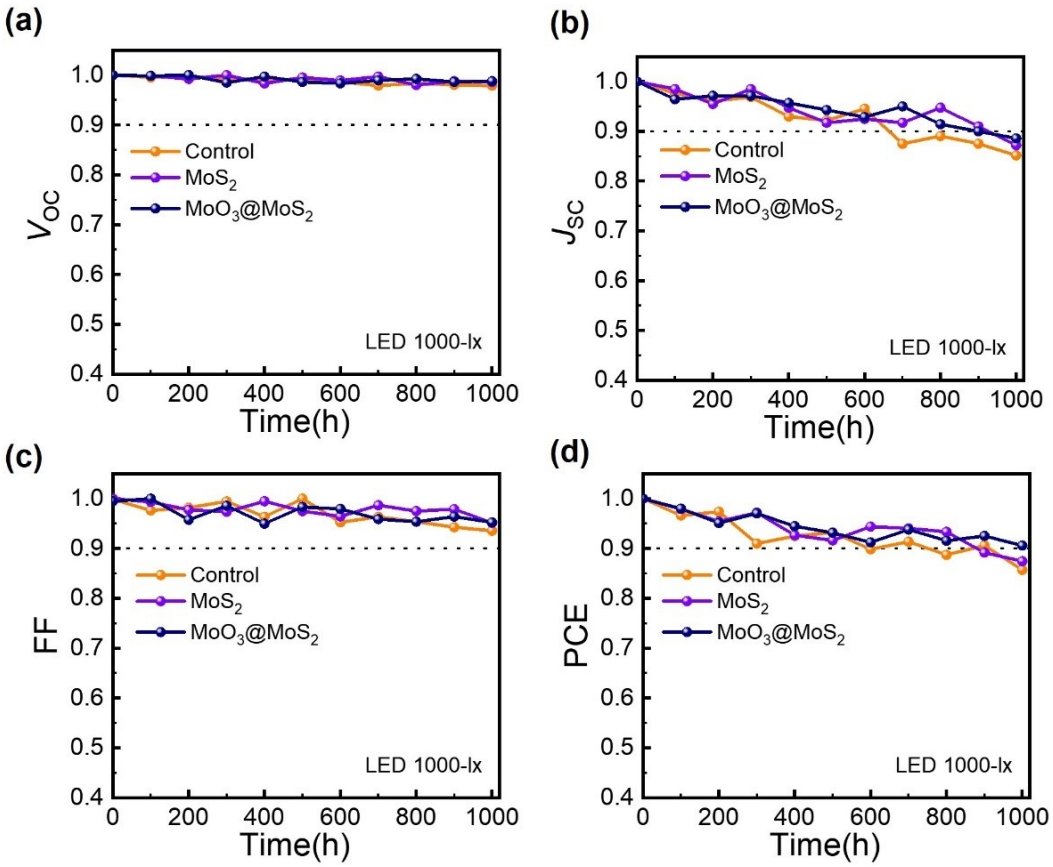

Figure S18. Stability of OPVs measured under LED illumination.

References

[1] Y. J. You, C. E. Song, Q. V. Hoang, Y. Kang, J. S. Goo, D. H. Ko, J. J. Lee, W. S. Shin, J. W. Shim, *Adv Funct Mater* **2019**, *29*, 1.

[2] H. S. Ryu, H. G. Lee, S. C. Shin, J. Park, S. H. Kim, E. J. Kim, T. J. Shin, J. W. Shim, B. J. Kim, H. Y. Woo, *J Mater Chem A Mater* **2020**, *8*, 23894.

[3] M. A. Saeed, T. H. Kim, H. Ahn, N. W. Park, J. H. Park, H. Choi, A. Shahzad, J. W. Shim, *Adv Opt Mater* **2022**, *2202135*, 1.

[4] Z. Chen, H. Yin, Z. Wen, S. K. So, X. Hao, *Sci Bull (Beijing)* **2021**, *66*, 1641.

[5] M. A. Saeed, S. Cheng, S. Biswas, S. H. Kim, S. K. Kwon, H. Kim, Y. H. Kim, J. W. Shim, *J Power Sources* **2022**, *518*, 230782.

[6] T. H. Kim, H. J. Lee, M. A. Saeed, J. H. Son, H. Y. Woo, T. G. Kim, J. W. Shim, *Adv Funct Mater* **2022**, *2201921*, 1.

[7] Z. Chen, T. Wang, Z. Wen, P. Lu, W. Qin, H. Yin, X. T. Hao, *ACS Energy Lett* **2021**, *6*, 3203.